RESEARCH ARTICLE | JUNE 08 2023

# Computational modelling of the selective laser sintering process FREE

João Castro; João Miguel Nóbrega ✉; Ricardo Costa



*AIP Conference Proceedings* 2997, 050001 (2023)
https://doi.org/10.1063/5.0159825

# Computational Modelling of the Selective Laser Sintering Process

João Castro [a)], João Miguel Nóbrega [b)] and Ricardo Costa [c)]

*Institute for Polymers and Composites, University of Minho, Campus de Azurém, 4800-058 Guimarães, Portugal*

[a)] joaoctcastro@gmail.com
[b)] Corresponding author: mnobrega@dep.uminho.pt
[c)] rcosta@dep.uminho.pt



**Abstract.** Additive Manufacturing (AM) has increased in popularity in numerous important and demanding industries due to the capability of manufacturing parts with complex geometries and reduced wastage. As one of its most popular techniques, selective laser sintering (SLS) is sought after by several industries that aim to replace conventional and more expensive processes. However, the SLS process is intrinsically complex due to the various underlying multi-physics phenomena and more studies are needed to obtain more insights about it. This has resulted in many academical interests to optimize the process and allow it to achieve industrial standards. Most of these optimization attempts are performed through experimental methods that are time-consuming, expensive and do not always provide the optimal configurations. This has led researchers to resort to computational modelling, aiming at better understanding the process to anticipate and fix the defects. The main objective of the present work was to develop a computational model capable of simulating the SLS process for polymeric applications, within an open-source framework, at particle length scale. Since distinct approaches are required for accurately simulating each step of the SLS process, different numerical methods were employed to develop a tool capable of studying the impact, in a representative section of the powder bed, of the physical parameters that can be adjusted in the process. The developed work comprises several steps, starting with an extensive study of the theoretical aspects of the SLS process, which aimed at the acquaintance with the underlying phenomena, process unwind, its parameters and their influence, as well as evaluating the existing limitations and challenges. This step was then followed by a detailed analysis of the most common employed models to represent the major phenomena and of the accuracy level of the approaches, based on the employed simplifications. A set of computational tools was then assessed and their built-in models were selected, when possible, according to the precedent literature review. Lastly, various tests were carried to obtain an experimental qualitative validation of the used code, to assure that the undetaken approach was adequate to simulate the process. The achieved developments represent a significant advance towards the detailed SLS process simulation. With the use of open-source software (LIGGGHTS e OpenFOAM), several studies were performed on a realistic powder bed section and, despite the absence of enough and more detailed experimental data, the simulation results are in agreement with the ones used for comparison. Overall, the accomplished work allowed to conclude that the employed tools constitute a great potential to study, in detail, the SLS process and its parameters influence and, therefore, contribute to its optimization.

## INTRODUCTION

### Additive Manufacturing

Additive Manufacturing (AM) is the formal designation for rapid prototyping and is commonly referred to as three-dimensional (3D) printing. AM is not a single process, but a set of technologies that share the characteristic of building parts layer-by-layer, which allows for more complex geometries and the production of objects with virtually any shape. Building in such a way removes the need of extra tooling and reduces material waste, since the only material used is the one present in the final part (except for support structures). Also, the dismiss of external tools or moulds makes AM processes a cheaper, faster and, therefore, viable option to produce parts in small

*Novel Trends in Rheology IX*
AIP Conf. Proc. 2997, 050001-1–050001-16; https://doi.org/10.1063/5.0159825
Published by AIP Publishing. 978-0-7354-4547-5/$30.00

quantities and prototypes, especially when considering how easy it is to iterate the design. The concept of layer-by-layer printing was used as early as the 19th century in areas such as topography and photosculpture [1] with simpler materials, such as cardboard and wax, inspiring the development of processes that would later result in modern AM techniques. Nowadays, AM is being applied in a wide range of relevant technological fields, such as biotechnology, aerospace, robotics, environment, energy, automotive and common industry [2]. The AM process comprises three main stages [3]:

1. The digital modelling of the part in a computer aided design (CAD) software and its conversion to a compatible format, generally the standard tessellation language (STL), which is sent to the AM machine;
2. Geometry manipulation by the machine to assure that it is oriented, positioned and sized correctly, as well as virtually sliced by horizontal parallel cuts, with a specified thickness, that represent the layers and work as guides for the printing stage;
3. The building process, which occurs mostly automatically, often just requiring superficial monitoring to avoid the occurrence of errors. When it ends, the part is safely removed and optional post-processing steps, such as removal of supports, dusting and sanding, are performed.

The printing and characteristics of a part vary significantly depending on which technology and process parameters are used for its manufacture. Different methods have distinct layer bonding strategies and ways to split and support them, meaning that equal, or very similar, geometries, result in dissimilar parts when different technologies, or machines within the same technology, are being used. Due to the large number of technologies based in AM, there are a variety of options when it comes to selecting a process. The same applies to materials, with polymers being the most popular due to their processability, low cost and unique properties [9, 10]. All these approaches, paired with the different materials used, will determine factors such as the printing speed, mechanical properties and accuracy of the final product [3].

## Powder Bed Fusion

According to the ASTM technical committee [4], powder bed fusion (PBF) is one of the seven main AM processes. It was one of the earliest developed and commercialized techniques and, nowadays, it remains one of the most versatile due to various possible energy sources, machine configurations, materials and ways to bind them together. The PBF process, as the name suggests, consists in the fusion of a powdered material that is in the machine bed. It can be divided into three main steps:

1. Powder recoating, where a new layer of material is spread evenly;
2. Energy input, which involves transfer of thermal energy from a heat source to the material;
3. Material coalescence and cooling, where granules fuse and subsequently cool to a solid state.

This process distinguishes itself from others within AM due to the use of high-density energy sources, such as lasers and electron beams, being the former far more common. It is a process that does not require support structures, since the non-melted particles act as integrated supports, which reduces material waste and allows for more complex designs. These particles can also be reused in different builds, a very attractive feature for economic and environmental reasons. This feature also facilitates the building of multiple parts in the same bed because the space required for supports is now free, thus increasing process efficiency.

The use of lasers within the PBF process is known as laser sintering (LS) and, depending on the main fusion mechanism, technologies employed and patent related problems, various names are given to this PBF variant. One of those is Selective Laser Sintering (SLS), a patented name given to LS that has been widely used in the field, being frequently found in articles replacing the term LS.

## Selective Laser Sintering

The SLS process, being a PBF technology, shares its already mentioned benefits. When compared to other popular AM processes, such as fusion deposition modelling (FDM), SLS offers much higher resolution, accuracy and surface finish quality, mainly because of the laser spot and particles small size [5]. Despite not being the process with better results, SLS is still the most popular amongst engineering applications because of the resulting parts mechanical properties and much faster printing speeds [5]. All these advantages led to SLS being increasingly used in important and demanding industries, such as automotive [6], aerospace [7] and biomedical [8].

A general representation of the SLS process is illustrated in Fig. 1. SLS machines are divided into two main zones, the build chamber, where the parts are built, and the feed chamber, which stores the necessary powder for the

process and provides it to the build chamber when needed. Although possible to use the laser to melt the material from room temperature, in SLS, the powder is pre-heated to a temperature just a few degrees below its melting point. Besides minimizing the laser power requirements and allowing a faster scanning speed, this reduces temperature gradients between scanned and non-scanned particles, facilitating the fusion between layers and keeping a more uniform temperature on the bed, which helps to prevent defects, such as local shrinkage and thermal distortions caused by non-uniform thermal expansions and contractions [9]. The pre-heating is done in bulk, being achieved through a combination of heat lamps and conductive elements above and around the perimeter of the build and feed chambers, respectively, and is maintained throughout the entire build process. Considering the possibility of the material thermal degradation due to these high temperatures during both the pre-heating and building phases, the process takes place inside a closed chamber filled with an inert gas, generally nitrogen, to minimize oxidation. After the pre-heating phase, the remaining steps of the process take place. Initially, the build piston starts at its highest position and a levelling roller spreads material from the feed supply to the build platform, creating the first powder layer. The amount of material dragged by the roller is always greater than the required for the layer, to assure that it is completely filled. When the layer is complete, a laser beam is directed to the powder bed through a set of lenses and guided to the desired positions, at a pre-selected speed, with the use of mirrors. As the laser spot moves, it scans the material, providing enough energy to melt and coalesce with adjacent granules, including the ones on the previous layer (if it exists). The unscanned powder stays in place and works as support for the next layer. After scanning the present layer, the build piston lowers the powder bed by the thickness of one layer and a new powder layer is spread on top. These operations are repeated until the desired object is fully built and, after that, the heaters are turned off and the part is left to cool inside the machine chamber, so the cooling is as uniform as possible and within an inert ambient. Once cooled, the part can be removed, cleaned off and, if necessary, subjected to finishing operations.

Despite being easy to understand the basics of the different process steps within SLS, it has been found that, when compared to other techniques, they are not as simple, accurate or reproducible as they may appear, especially for thermoplastic parts [10]. That is because LS processes are intrinsically complex due to the various underlying multi-physics phenomena, therefore, more efforts are needed to obtain more insights about the process. Some of the main known limitations are associated with the shortage of compatible or appropriate materials and the knowledge and skills in a wide range of fields. Furthermore, there are still a significant amount of process deficiencies that have not been fully eliminated due to its complexity, such as pores and microcracks [11], curling [12] (the combination of both shrinkage and warping) and distortion caused by residual stresses [13]. Most of these defects are a direct outcome of the accentuated temperature gradients induced during the heating and cooling cycles and, considering the amount of recent publications related to the topic, significant efforts are being put into solving them. Fixing problems via trial-and-error experimental methods takes a vast amount of time, is expensive, does not allow

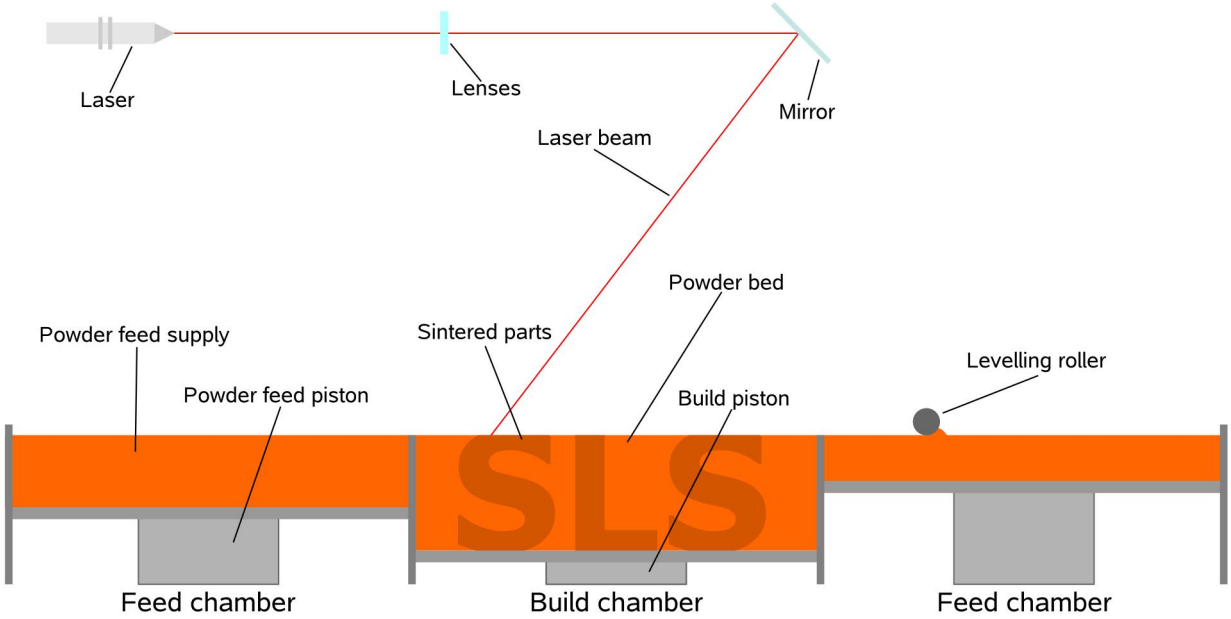


**FIGURE 1.** Schematic representation of the SLS process.

obtaining detailed information on the temperature profiles or stress fields nor assess the identification of the optimal configurations. For these reasons, researchers have been resorting to computational modelling, aiming at better understanding the process to anticipate and identify ways to fix the defects without manufacturing physical prototypes.

## State-of-the-Art

Although it is possible to build a part using LS technology without simulating the process beforehand, that does not mean that it is not necessary or recommended. When building simple prototypes, the mechanical properties or visual appearance might not play a relevant role, however, when manufacturing parts with demanding requirements, those tend to be very important. Accordingly, simulating the process beforehand is useful to predict errors and provide technicians with important insights to better understand the process, which might lead to optimizations on part design and process parameters.

There are different approaches employed for numerical simulations, which can be classified into two major groups: mesh-free and mesh-based, with the last being much more popular. Mesh-free alternatives are based on discrete element method (DEM), lattice boltzmann method (LBM), optimal transportation method (OTM) and smoothed particle hydrodynamics (SPH), while mesh-based counterparts comprise the finite element method (FEM), the finite difference method (FDM) and the finite volume method (FVM). The DEM is the most common mesh-free method employed for simulating the process, but mainly for the powder bed distribution [14]. It accounts for the discrete nature of the powder bed and considers the interactions between each particle at their contact point, being well suited for the study of granular media. Despite its elementary Newtonian mechanics, it has been extended to include other interactions between particles, such as heat transfer [15], that allowed the temperature distribution study within a realistic powder bed [16]. Unfortunately, this approach fails to consider the surrounding air or the fusion and coalescence of the particles. On the other end, mesh-based methods, such as the FEM, firstly introduced in 1956 [17], stands out for its extensive use for simulating the SLS process [18-20] due to its simplicity, efficiency and mainly the vast amount of literature on the subject over the past decades. Even though it provides useful information, such as the temperature evolution, liquid fraction and residual stresses, this method makes it difficult to account for volume shrinkage, layer deposition and the particle nature of the bed [21], which motivates some authors to opt for the FVM [22]. Also, since meshed-based methods turn out to be more cumbersome to simulate the powder distribution and deposition, DEM is often coupled with those approaches to take care of this step [23].

Unlike conventional manufacturing processes, such as injection and extrusion, whose process have been extensively studied and optimized in the past, the optimization of the SLS process is more recent. It is usually performed through experimental methods [24], but such approaches are time-consuming and expensive. The primary purpose of most simulations on the SLS process is to assess the influence of the various process parameters into the final part mechanical and geometrical quality. Although the process being the same, distinct modelling approaches are taken for different materials, mainly polymers and metals, due to their different behaviours. For example, metals are exposed to a much wider temperature range, so considering their temperature dependent properties is imperative [25]. Also, due to their reduced viscosity, liquid metal flows are heavily influenced by density variations and many other effects that need to be accurately modelled [26]. The numerical modelling of temperature distribution, deformation and thermal stresses of a SLS process is similar to that of multi-pass welding [27], which is an older technology that has been developed and modelled for more than four decades. Unfortunately, for the SLS process, the model has to be more advanced due to all the additional complex physical phenomena involved, such as the laser interactions with the powder, namely absorption, reflection and scattering. Despite being a relatively new technology, there was already a significant number of attempts to simulate the process. Some approaches aimed at developing a model and validating it by comparing simulation results with experimental ones [28], while others aimed at optimizing a process or study the influence of certain parameters. Considering the powder bed as a continuous media, Childs et al. [29] investigated the influence of laser power and scanning speed and Dai and Shaw [30] the influence of scanning pattern and speed on the temperature and stress fields. Bugeda et al. [31] also developed a model to simulate the 3D sintering process of a single track, obtaining data such as the temperature field, solid fraction and sintering depth. Similarly, Dong et al. [32] modelled the transient heat transfer during the sintering process while considering the phase transition, but also the temperature dependent material properties to evaluate the temperature and density distribution. A more accurate model, considering a more realistic volumetric heat source, was developed by Riedlbauer et al. [33] to predict melt pool dimensions and validate the results with experimental data. Still related to melt pool, Peyre et al. [34] and Foroozmehr et al. [35] tested the effects of the process

parameters on its temperature distribution and dimensions, validating the results with experimental tests. Bierwisch et al. [36] developed a 2D model with a realistic powder bed for two different materials, where the various phases of the process, namely scan, heat dissipation and cooling, were considered. Osmanlic et al. [37] developed a similar model with an accurate laser source, where phenomena such as reflection, refraction and attenuation were considered, but for much shorter time scales and with the objective of assessing the bed density influence on the process. Some authors compiled and reviewed several studies [26, 38-41] and the interested reader is addressed to those publications to obtain further details. Besides isolated models, there are also some proprietary software that offer the option to simulate the LS process, such as ANSYS [42], SIMULIA [43], COMSOL [44] and NETFABB [45]. Also, for DEM simulations, LIGGGHTS [46] and LAMMPS [47] are commonly used.

Modelling SLS processes comes with several challenges. There are non-linearities to be considered, such as the temperature dependence of the material properties. Besides that, the problem must be discretized both spatially and temporally and, depending on the model scale, very small time scales and high mesh resolutions might be needed, which requires a significant computational power. For the interaction of the laser with the material, there are several different physical behaviours to consider, such as absorption, reflection and radiation, along with the subsequent heat transfer, phase transformation, moving interface between the different phases, fluid flow and possible chemical reactions. Moreover, the powder distribution also affects most of the previously mentioned aspects, so an adequate geometry definition is also needed. In the end, for an accurate AM simulation, one must model the addition of the material, have a realistic model for the heat source, account for the thermal losses, consider the temperature dependence of some properties, model elasto-plastic stresses and strains, couple the thermo-mechanical behaviour in a manageable way and, finally, model phenomena that change material properties [48]. However, these requirements are computationally demanding, therefore it is important to investigate whether simpler models are also able to provide useful insights about the process.

## COMPUTATIONAL SETUP

### Powder Bed Formation Simulation

The first step towards preparing the simulation is to build the computational geometry, in this case, the powder bed, which will be incorporated the simulation domain, later. For the detailed analysis of the various process parameters influence on the sintering evolution, the scale of the problem must be at the particle length and the powder distribution should be as realistic as possible, so that the final results are representative of reality. To reach the indicated standards, LIGGGHTS [46], a DEM particle simulation software, was used. The main objective of the LIGGGHTS simulation is to obtain a representative section of the powder bed and then generate a computational mesh that will be used later with the CFD software. Performing a simulation of the formation of an entire powder bed would be very time-consuming given the large number of powder particles in it. Even a single layer would be too large considering that a small representative section is enough to accomplish the objectives. Thus, only a portion of the bed was simulated during the deposition of one layer, as illustrated in Fig. 2. The dimensions of this section were selected to accommodate, in thickness, approximately two layers of material, and a surface area that allows the crossing of two consecutive laser scans.

For the simulation, two geometries, a box and a blade, that are displayed, together with their dimensions, in Fig. 2a, were created using a CAD software. Both act as walls, which means that particles collide with them without getting through. The box has a deeper section that can be viewed as a smaller box under the larger one, where the particles will fall, simulating the deposition of one layer. This smaller box will contain the representative section of the powder bed. The first step in the simulation is the particles insertion that lasts for two seconds and takes place over an area in the far end of the larger box (Fig. 2b). It is then followed by the blade movement, that moves at a constant speed in the $x$ direction. Before the inserted powder reaches the smaller box, it has to be dragged over a long flat section that was purposely made in such way, not only to accommodate the particles insertion, but also to assure a more realistic powder distribution because, this way, the particles are packed by the blade movement and their "flow" is more developed before falling into the hole (Fig. 2c). Once past the smaller box, the blade will keep moving, dragging the remaining particles past the boundary, outside the simulation domain, deleting them (Fig. 2d). At the end, only the particles inside the smaller box will be used for the mesh generation.

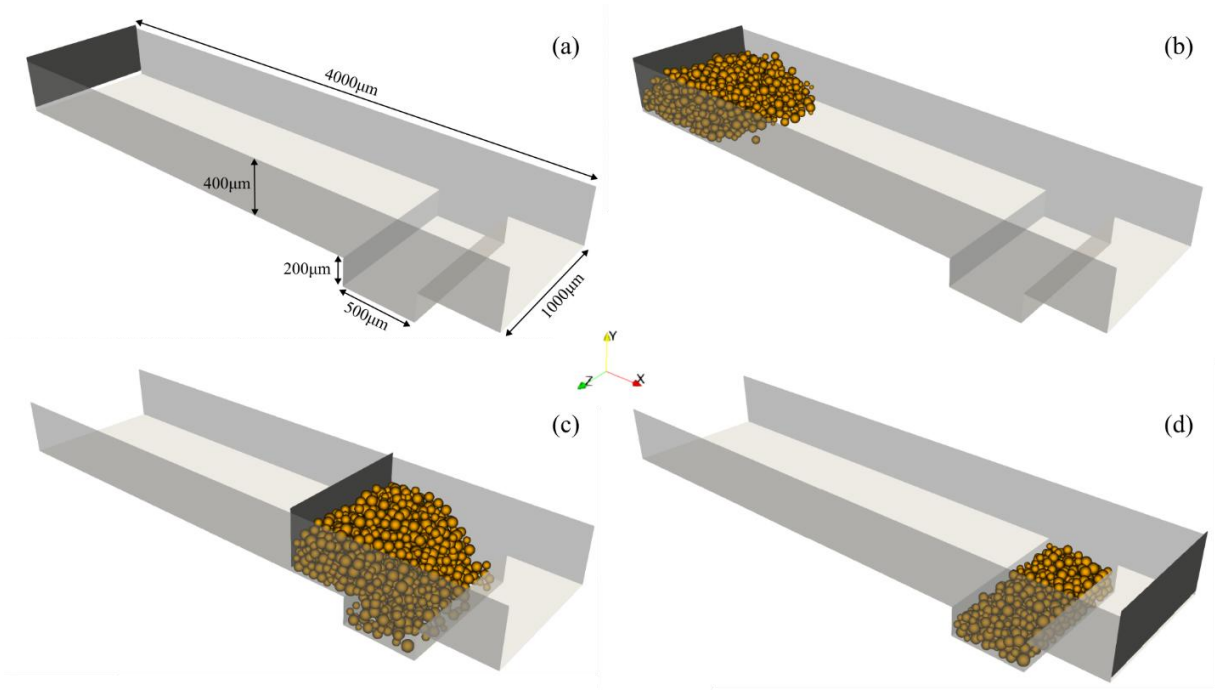


**FIGURE 2**. Various stages of the powder bed representative section formation simulation.

## CFD Solver

The icoReactingMultiphaseInterFoam solver was originally released with OpenFOAM version 1806 [49]. It is a subcategory of the multiphaseInterFoam solver that, itself, is based on the parent solver interFoam, which solves the continuity and momentum equations for two fluids with a phase fraction that is tracked resorting to the Volume of Fluid (VOF) algorithm [50]. multiphaseInterFoam follows the same principles, but for multiple incompressible fluids, tracking phase fraction, while also considering surface tension and contact-angle effects for each phase [51]. Being a subcategory of these solvers, icoReactingMultiphaseInterFoam shares many features, but was complemented with additional functionalities. For instance, it allows the user to choose the thermodynamic model for each phase, but the main assumption of the shared fields among the phases from interFoam, namely velocity, pressure and temperature, remains. The solver supports mass and heat transfer between different phases of the same material, similar to the ones on which it is based, but also allows it between different phases of the distinct materials.

Among the many solvers present in the OpenFOAM library, the icoReactingMultiphaseInterFoam was selected because it meets the modelling requirements for the SLS process, such as modelling the polymers phase change, considering fluid flow and taking into account interactions between multiple phases, including interface tension forces. The solver also contains a laser radiation model capable of modelling a volumetric heat source, following a Gaussian distribution that attenuates as it passes through the material. Previous work was also done to explore and assure the solver capability to simulate the SLS process [52], which further reinforces its selection to model the problem of interest.

## Material Properties

The selected solver considers each state of the material as a separate phase and requires the specification of its properties separately. For this case, a total of three phase files should be provided: *alpha.solid*, for the initial solid polymer, *alpha.liquid*, for the polymer in liquid state and *alpha.air*, for the surrounding air present in the chamber.

Accurately defining the properties for polymeric materials is challenging because of their intrinsically complex behaviours. Most properties, in order to be accurately determined, require the replication of the SLS process conditions that are hard to achieve, or obtained through unconventional characterization methods, which leads to less adequate information available. Moreover, polymer properties heavily depend on the surrounding conditions,

namely the temperature, and the increase in temperature during the process causes the material to age, a phenomenon that will change its properties. The polymer utilized is a widely used polyamide for SLS applications, PA12 - PA 2200, produced by EOS [53]. Among the list of parameters that the solver can work with, the useful ones for the simulation, provided in Tab. 1, are the density, specific heat, thermal conductivity, viscosity, surface tension, melting point, complex index of refraction and coefficient of absorption for the laser. All the properties were defined as constant, mainly due to the lack of information to specify them otherwise, except for the specific heat, that requires a different treatment, since the solver does not take into account the enthalpy of fusion, which would help into more accurately accounting the total energy required for phase change. Fortunately, preliminary tests were performed on the material that allowed the determination of the specific heat as function of the temperature, which is expected to greatly increase the accuracy of the simulation. Within the temperature range of interest, the values were introduced in the form of a table. Additionally, not considering the enthalpy of fusion brings an additional challenge for selecting the melting point. Polymers do not have a well-defined melting point, but instead, melt over a range of temperatures. The solver does not consider such behaviour and the material will change phase when it reaches the transition temperature. In reality, one tends to consider the beginning of the melting range, also known as onset of melting, as the melting point that, for this material, is 449.15 K. Doing that for the simulation is inaccurate because it would be largely over predicting the amount of liquid phase, since it would consider as fully liquid any solid cell above that temperature. Due to these reasons, the selected phase transition temperature is somewhere in between those two, at the peak energy point during the DSC test, commonly referred to as simply the melting temperature, with the value of 461.75 K [54]. More information, regarding the material properties, is available in the preceding work in which this publication is based [52].

**TABLE 1.** Polymer properties for the computational studies.

| Property | Value | Units |
|---|---|---|
| Density | 1000 | $kg/m^3$ |
| Thermal Conductivity | 0.2 | W/(m K) |
| Viscosity (at 474k) | 390/5095 | Pa/s |
| Surface Tension | 0.035 | N/m |
| Absorption Coefficient | 1.3x104 | $m^{-1}$ |
| Complex Index of Refraction | 1.6+ *i*0.011 | - |

As for the atmosphere, the chamber is filled with an inert gas, usually nitrogen, in order to avoid degradation reactions, such as oxidation. Even though a significant amount of information was found regarding the temperature dependency of the nitrogen properties, they were all defined as constant to simplify the model and the calculations. Besides that, the material at study is the polymer so, as long as the gas properties are close to their real value, it should not drastically influence the results. The values for the density [55], thermal conductivity [56], specific heat [57] and viscosity [58], for temperatures within the process range, were all obtained from well-known material databases. For the absorption coefficient, no information was found regarding its value for the employed laser, however, a study for other gases, with a CO2 laser beam at a close wavelength value, showed that the absorption coefficient for gases is much smaller and almost negligible [59]. Since no study on the process mentions the interaction of the laser with the air, it was assumed that it was insignificant, therefore a small value was selected. The gas properties considered in the studies are provided in Tab. 2.

**TABLE 2.** Atmosphere properties for the computational studies.

| Property | Value | Units |
|---|---|---|
| Density | 0.676 | $kg/m^3$ |
| Thermal Conductivity | $3.887x10^{-2}$ | W/(m K) |
| Viscosity | $2.6x10^{-7}$ | Pa/s |
| Specific Heat | 1049 | J/kg K |
| Absorption Coefficient | 1 | $m^{-1}$ |

## Surface Tension Studies

The surface tension is the driving force for the coalescence between particles, which makes it extremely important for the process dynamics. Such crucial mechanism has to be accounted for in the model and its behaviour needs to be studied before advancing with more complex simulations. To test the model, two spheres with a

diameter of 50 μm (the average particle size) were positioned inside a domain where they are only in contact with each other. To isolate the studies, all optional models are disabled and the spheres already start in a liquid state at a uniform temperature. While keeping the surface tension constant with a value of 0.035 N/m, two different viscosities were employed in distinct tests, 390 and 5095 Pa·s. The values are, respectively, from the virgin and used material.

*Virgin Polymer*

The results from the tests with the virgin material, illustrated in Fig. 3, show a complete coalescence between the two particles after five seconds, which, considering that the building process lasts much longer, is a fast consolidation. Unfortunately, no information was found regarding the sintering time between two particles that allowed for a comparison with the obtained results, however, a study on the sintering evolution between two particles of PA2200 by slowly increasing their temperature is illustrated in Fig. 4 [60]. Despite the absence of a time scale, it is possible to analyse and compare the evolution of the particles shape and the neck that they form. Fig. 4a shows the particles forming a very small neck, in a stage slightly before what is visible after 0.25s on the simulation. At Fig. 4b, the neck is further developed and the shape similar to the results at 0.5s. Lastly, in Fig. 4c, the two particles are now a single one with an oval shape that resembles the results at 2s.

*Used Polymer*

The tests with the used material (Fig. 5) differ significantly from the previous ones. The used material viscosity is more than ten times higher, which highly hinders the displacement of the liquid phase. For these results, a different time scale had to be considered, since it took three seconds for the neck formation to be similar of just a quarter of a second with the virgin material. In this case, the much larger viscosity does not allow for a quick development of the neck and, instead, the particles coalesce partially by attracting themselves.

*Mixed Properties*

As previously noted, during the process it is expected that the material properties are modified, namely an increase in viscosity, due to exposure to high temperatures. There is usually a mix between the used powder and the

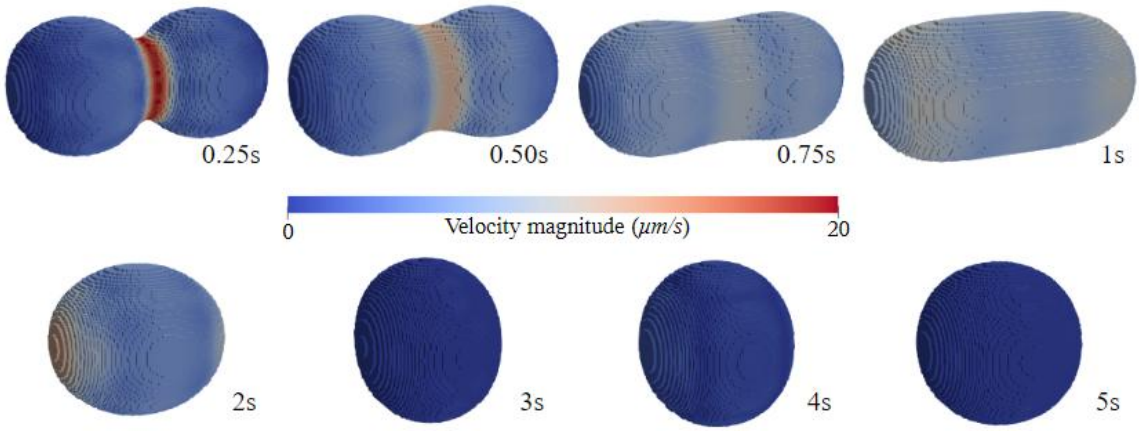


**FIGURE 3**. Surface tensions studies with virgin material.

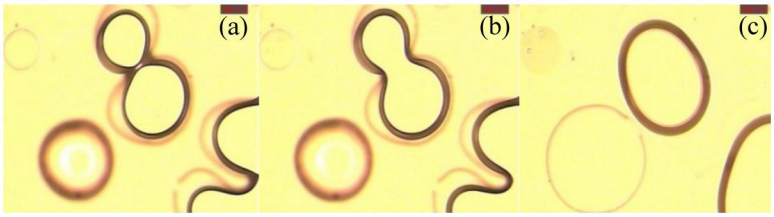


**FIGURE 4**. Hot stage microscopy of PA12 - PA2200 (adapted from [60]).

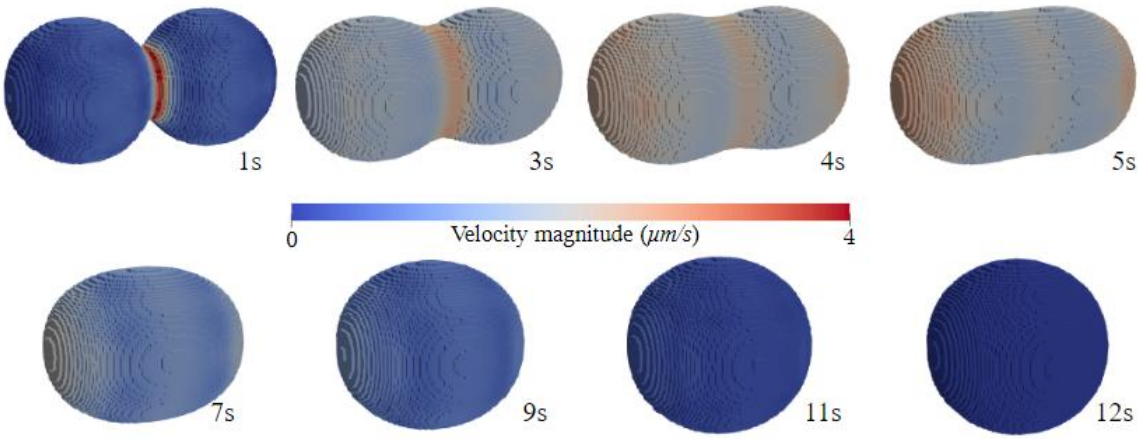


**FIGURE 5**. Surface tensions studies with used material.

virgin one in an attempt to diminish the negative effects of ageing. In reality, the powder bed would contain a percentage of each type of particles, virgin and used, that have distinct viscosity levels. For an appropriate case setup, this would require two distinct liquid phases with their respective properties. However, because the solver was developed for immiscible liquids, distinct phases would not mix and the behaviour would not be a realistic representation of the process. Due to the impossibility of adapting the code, in a reasonable time frame, to fit the specified needs, the material properties were considered, for simplification, as a pure mixture of virgin and used material, with an average viscosity of 2742.5 Pa·s. The coalescence development with this assumption is shown in Fig. 6. As expected, the sintering progression falls somewhere in between the virgin and used material cases, stabilizing their shape after approximately twelve seconds.

## ASSESSMENT STUDIES

The experimental cases that are going to be used as a reference are from an in-house process and are available in an article containing information on the process parameters, as well as the respective results at a microscopic level [61]. In this article, a complex geometry with various details was produced for dimensional and geometric evaluation. Among those details, there are squared structures with ten millimetres sides and various heights. Because these structures were later analysed in the article, the simulated representative section was assumed to be at the centre one of those. In these studies, the geometry will be scanned by two adjacent lines and the particles inside the scan area will be analysed. Three different cases, from the article of reference, with low, medium and high energy parameters, will be used as a base for comparison. The only differing variables between tests will be the laser power (17.1, 30.0 and 38.7 W, respectively) that will be selected according to the study. A vertical cross section of the scanned part for each case, which will be used later to compare with the simulation results, is illustrated in Fig. 7.

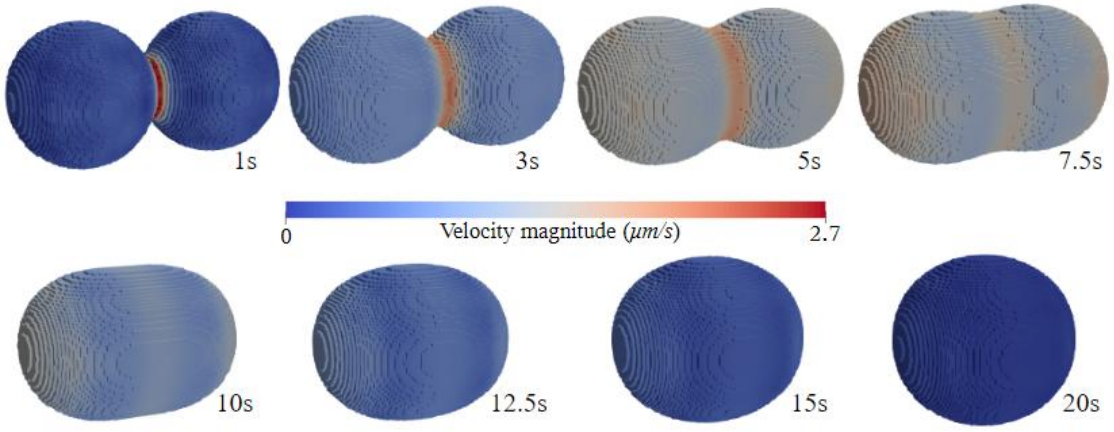


**FIGURE 6**. Surface tensions studies with mixed properties material.

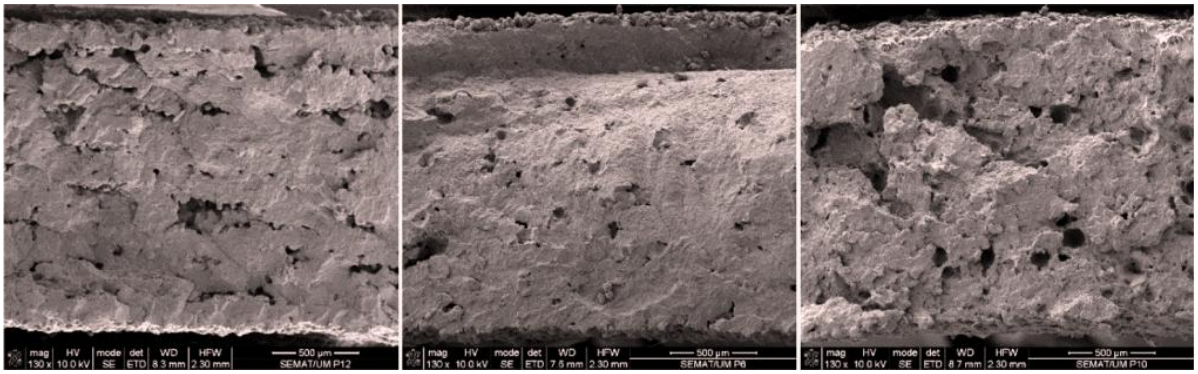

**FIGURE 7**. Cross section of samples obtained with low (left), medium (middle) and high (right) energy parameters (adapted from [61]).

The powder bed representative section was inserted in a meshed box with boundaries adjacent to its limits. The initial and boundary conditions were selected in a way that would better replicate the process considering the smaller scale of the problem. Starting with the temperature, since the performed studies aim at evaluating the process evolution during and after the laser scan, the temperature conditions are those of the bed after the pre-heating phase, at 446.15 K. To avoid imposing large temperature gradients at the boundaries, the lateral and bottom boundaries were defined with a null gradient condition. The top patch, because it is not in contact with the spheres, was kept constantly at the initial temperature, since natural convection is expected to redistribute energy to the large process chamber. For the velocity conditions, initially the entire domain is stationary. As for the boundaries, a null velocity gradient was imposed at the boundaries to prevent particles sticking to them, with the obvious exception of the bottom patch that was treated as a wall, otherwise mass would fall outside the domain due to gravity. The representative section is inside an unpressurized chamber, therefore both the internal cells and boundary faces are initialized with atmospheric pressure values. Lastly, the absence of inlets in this problem simplifies the boundary conditions for the phase fraction of all phases to a null gradient.

## High Energy Case

The experimental test case with high energy parameters lead to the degradation of material, as it is clearly visible in the right image in Fig. 7, by the burned aspect of the material and large holes present in the cross section.

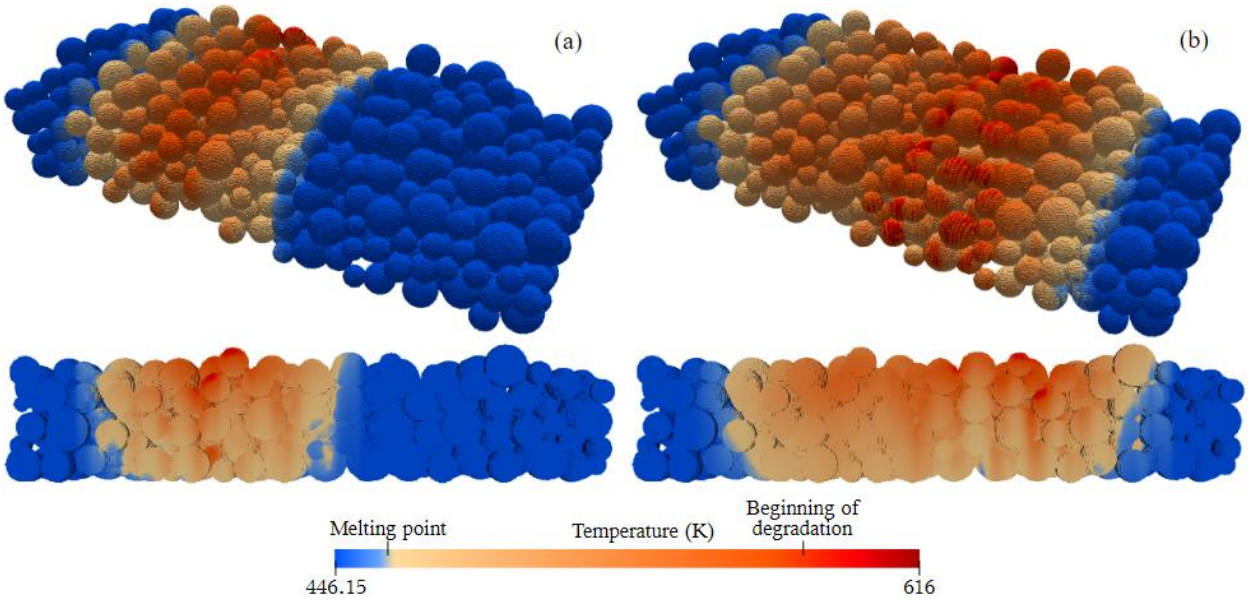


**FIGURE 8**. Temperature distribution after the first (a) and second (b) laser scans for the High Energy case.

Unfortunately, the current solver is not equipped with a degradation model, but validation can be performed by comparing the material temperature profile after the scan. The simulation results, displayed in Fig. 8, show that, with the corresponding process parameters, there is, indeed, an excessive amount of energy. Considering that the geometry contains approximately two layers of material, the energy transferred to the material is enough to fully melt both immediately. Besides that, looking at the temperature scale, every zone in red, or with a reddish tone, is above the temperature for the beginning of degradation of 574.15 K, that was taken from a TGA test. Degradation seems to be more prominent at the powder bed surface, especially where the two subsequent scans overlap, as visible in Fig. 8b. The experimental results do not show major degradation, which indicates that the material did not reach the onset of degradation of 669.6 K and was, most likely, closer to values where the degradation rate was much less accentuated. Based on such comparison, it seems that the temperature profile obtained in the simulation is close to the experimental observations.

## Medium Energy Case

For the Medium Energy case, looking at the simulation results in Fig. 9, one can conclude that the provided energy is more than enough to fully melt the scanned zone for one layer, with plenty still remaining to reheat the previous one for a good layer adhesion. Compared with the high energy case, by lowering the power by 22.5%, the maximum temperature lowered by 45 K, just a few degrees over the beginning of degradation. The experimental results do not exhibit any signs of degradation, only an almost fully dense region with minor porosity from, most likely, powder bed formation defects. This implies that the material achieved high temperatures that promoted fluid flow, by lowering the viscosity, and allowed the particles to coalesce easier. Judging by the impossibility to detect layer separation, the energy provided must also have been enough to reheat the previous layers, which lead to a good layer adhesion. The numerical results, based on the temperature profile after scan, reasonably match the experimental ones.

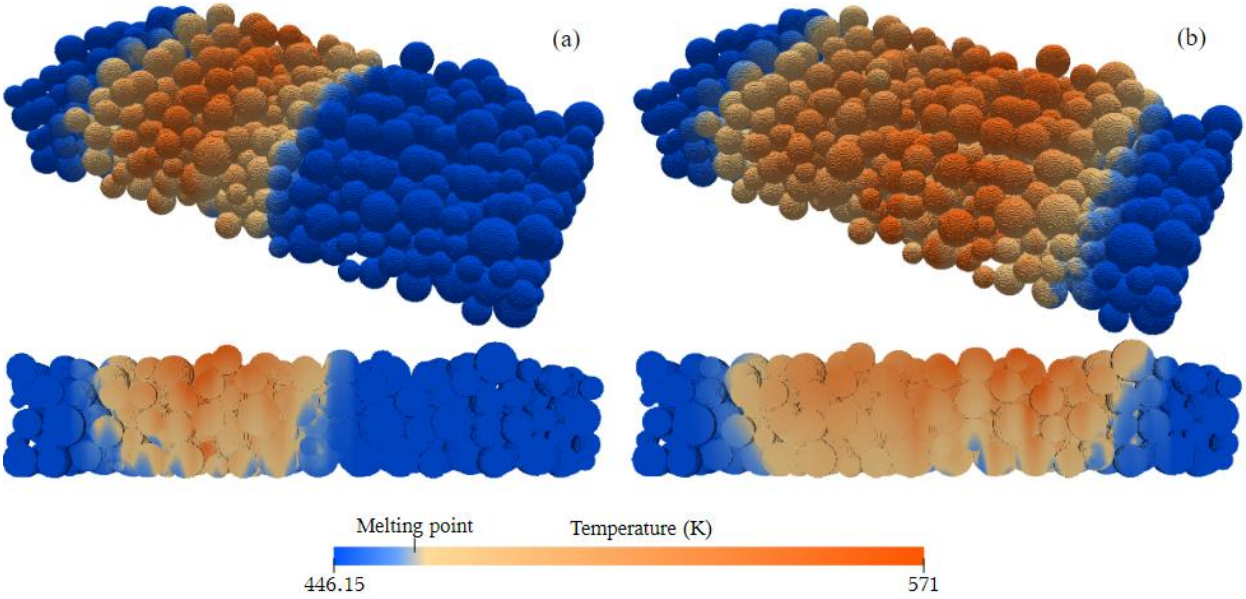


**FIGURE 9**. Temperature distribution after the first (a) and second (b) laser scans for the Medium Energy case.

## Low Energy Case

The last case (Fig. 7 (left)) has a significant decrease in laser power and, consequently, energy density. After analysing the experimental results, one can conclude that the diminishing energy clearly affected the built part since there is poor adhesion between some interlayer sections. Nonetheless, most of the cross section is fully dense and no unmelted particles are visible, which denotes that the lack of coalescence in the defective zones might be related to something else. The numerical results for the representative section temperature profile after the laser scan, visible in Fig. 10, are in agreement with what was mentioned in the previous paragraph. There is, indeed, enough energy to

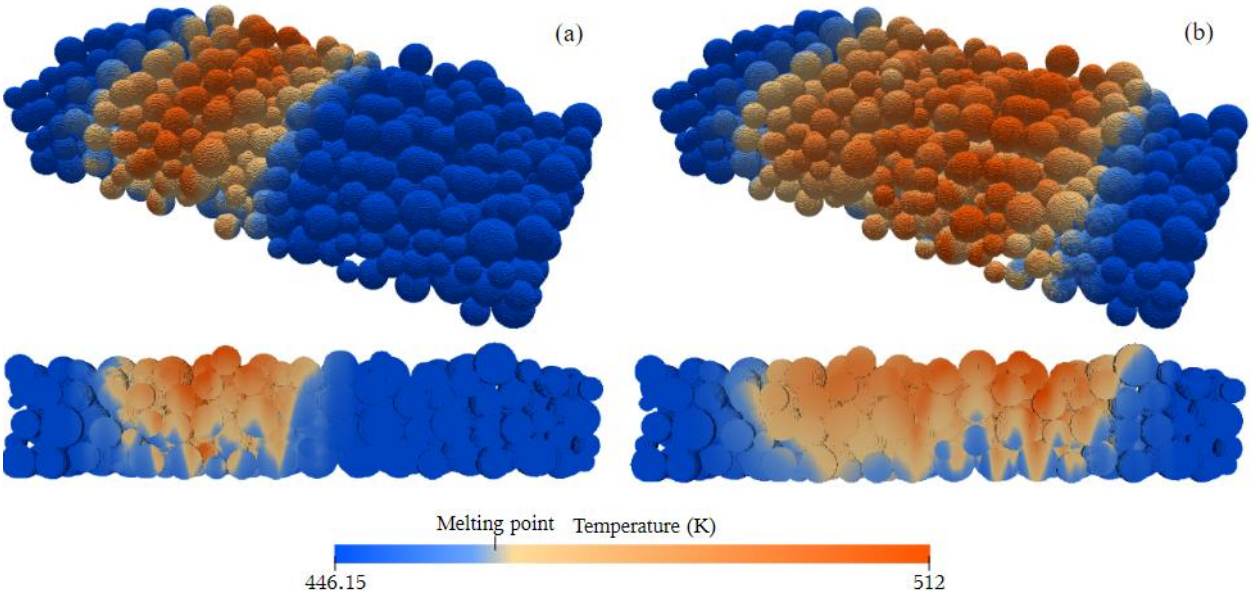


**FIGURE 10**. Temperature distribution after the first (a) and second (b) laser scans for the Low Energy case.

effectively melt one layer and reheat a significant portion of the previous one. However, due to the notable power decrease, the melt depth and overall temperatures are now much lower. Since, in this case, contrarily to the previous ones, the energy transferred to the material is insufficient to melt the entire section thickness right after the scan, the simulation was left to run until the remaining particles either melt by heat conduction, or the overall temperature reaches an equilibrium. After just two seconds, the dissipated heat was enough to melt the bottom of the section, as observed in Fig. 11. One could argue that, if the entire section (that represents two layers) is fully melted, poor layer connectivity should not exist, after all, the particles are liquid and will remain in that state until the cooling phase. In the simulation, because the viscosity is set as a constant and has a value between the virgin and used polymer, that would be the outcome. In reality, however, such simplifications do not apply. Starting with the powder mixture, half of the material is guaranteed to be virgin, while the remaining half is used, which is a very vague definition, since it does not specify how many hours or cycles each portion has. This entails that, among the used particles, different levels of viscosity are possible. Besides that, the surface tension, also set as a constant in the solver, decreases with material use [62], further contributing to a reduced coalescence. Additionally, and most likely the main reason for the poor interlayer coalescence in some regions, the viscosity levels decrease exponential with increasing

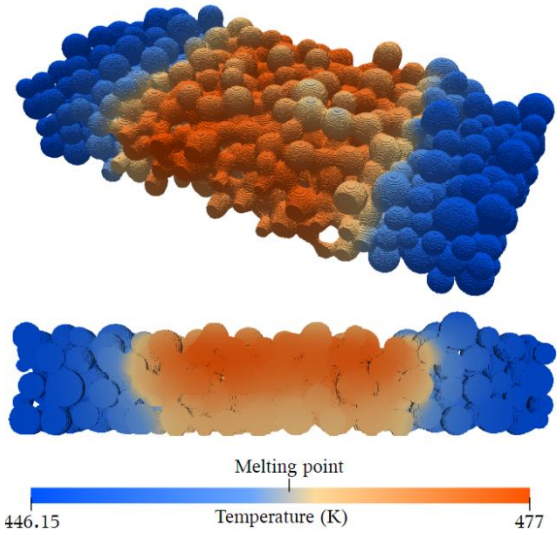


**FIGURE 11**.Temperature distribution two seconds after the scan for the Low Energy case.

temperature [63], which means that, although being liquid, particles that receive more energy will coalesce more and faster. In fact, by comparing only the experimental results with low and medium energy, it is safe to assume that both would contain formation defects and particles with high viscosity levels, still, in the medium energy case, the material, because it reaches much higher temperatures that greatly reduce its viscosity, is able to effectively coalesce into an almost fully dense part. Taking that into account, when analysing the simulation results, the molten zone, after just three seconds, has a maximum temperature of 474K on the core of the first layer that, coincidently, corresponds to the temperature at which the viscosities for both the used and virgin material are known. Below and around that zone, the temperatures are considerably lower thus the viscosity will greatly increase. Despite the lack of information on the temperature dependent viscosity and its implementation in the model, the temperature profile on the simulation results, considering what was discussed, present the same behaviour as the experimental counterpart.

## CONCLUSION AND FUTURE WORK

SLS is one of the most popular AM techniques due to its capability of processing parts with complex geometries and good mechanical properties with almost no material wastage. However, the process is extremely complex due to its multi-physics nature and, as a consequence, it is yet not fully understood. There is still a significant amount of defects associated with the process and solving them experimentally has proved to be challenging, expensive and time-consuming.

The present work focused on a global view of the SLS process and its simulation, with various aspects related to the process description, challenges and modelling discussed in more detail. Such analysis was necessary for the correct development of a computational tool to simulate the process at a particle length scale within an open-source simulation framework. By using LIGGGHTS and OpenFOAM, a realistic powder bed was created and several studies were performed to assess the process evolution. Among the various studies, despite some necessary simplifications, the results were very satisfactory and in agreement with the available experimental data used for comparison. Starting with the thermal model, the laser source is behaving as expected and, based exclusively on the temperature profile after scan, the temperatures achieved by the material are a good representation of the real behaviour. Regarding the coalescence, arguably the most important phenomena in the process, several simplifications had to be considered. Starting with the viscosity of the material, it was not possible to consider a portion of the particles with distinct viscosity levels to fully replicate the experimental practice, due to the incorrect interaction, predicted by the solver, between distinct liquid phases, thus, an average value had to be selected. Moreover, due to the lack of appropriate data, the viscosity was defined as constant, when, in reality, it varies significantly with temperature. By adapting the code and obtaining information on the temperature dependency of the viscosity for both the used and virgin material, a mixed powder bed could be used and the insufficient coalescence between particles, due to their high viscosity in low temperature zones, would be much more prominent and representative of the reality. Similarly, the surface tension is also treated as a constant in the current model, but if a temperature dependency was implemented, the results would likely also be more realistic. Sadly, no experimental data exists for that dependency as well.

Lastly, as a closing statement, the developed strategy, using exclusively open-source software, manifests an immense potential. The powder bed is a realistic representation of reality and the particle size distribution influence is clearly visible in the test cases. For a future work, if efforts are put into accurately determining the material properties that could not be correctly defined and the model is adapted to accept some dependencies and behave correctly between two distinct fluids, the current methodology could become an even more powerful tool to further assess, with higher detail, the process parameters influence. Moreover, for further validation of the solver capability, experimental cases with specific conditions, that would allow a more rigorous comparison with the simulation results, could also be performed.

## ACKNOWLEDGEMENTS

This work was funded by National Funds through FCT - Portuguese Foundation for Science and Technology, Reference UID/CTM/50025/2019 and UIDB/04436/2020, and project SIFA - Sistema Inteligente de Fabricação Aditiva (POCI-01-0247-FEDER-047108). The authors also acknowledge the support of the computational clusters Search-ON2 (NORTE-07-0162-FEDER-000086) and Minho Advanced Computing Center (MACC).

## REFERENCES


1. D. Bourell, J. Beaman, M. Leu and D. Rosen, Workshop On Rapid Technologies **24**, 5-11 (2009).
2. T. Wohlers and T. Gornet, Wohlers report 2015, 1-35 (2015).
3. I. Gibson, D. Rosen and B. Stucker, "Powder Bed Fusion Processes," in *Additive Manufacturing Technologies: 3D Printing, Rapid Prototyping, and Direct Digital Manufacturing*, (Springer, New York, 2015), pp 107–145.
4. F42 Committee. Terminology for Additive Manufacturing Technologies. ASTM International.
5. 3D Printing Technology Comparison: FDM vs. SLA vs. SLS, Available online: https://formlabs.com/blog/fdm-vs-sla-vs-sls-how-to-choose-the-right-3d-printing-technology/ (Accessed on 20 January 2023).
6. 3D Printing Now Good Enough for Final and Spare Car Parts, Available online: https://www.designnews.com/materials-assembly/3d-printing-now-good-enough-final-spare-car-parts (Accessed on 20 January 2023).
7. Airbus Helicopter: Cabin Ventilation Distributor | Prodways, Available online: https://www.prodways.com/en/airbus-helicopter-cabin-ventilation-distributor/ (Accessed on 20 January 2023).
8. New Jersey Man Receives 3D Printed PEEK Skull Implant - 3DPrint.com | The Voice of 3D Printing / Additive Manufacturing, Available online: https://formlabs.com/3d-printers/fuse-1/ (Accessed on 20 January 2023).
9. D. Bourell, T. Watt, D. Leigh and B. Fulcher, Physics Procedia **56,** 147-156 (2014).
10. J. Kozak and T. Zakrzewski, "Accuracy problems of additive manufacturing using SLS/SLM processes", in *XIII International Conference Electromachining 2018,* AIP Conference Proceedings 2017, edited by T. Paczkowski and R. Polasik (AIP Publishing, Melville, NY, 2018), pp. 020010.
11. D. Stoia, E. Linul and L. Marsavina, Materials **12**, 871 (2019).
12. A. Mousa, Rapid Prototyping Journal **22**, 405-415 (2016).
13. K. Manetsberger, J. Shen and J. Muellers, "Compensation of Non-Linear Shrinkage of Polymer Materials in Selective Laser Sintering," in *International Solid Freeform Fabrication Symposium 2001,* (University of Texas at Austin, Texas, 2001), pp. 346-356.
14. H. Chen, Y. Chen, Y. Liu, Q. Wei, Y. Shi and W. Yan, International Journal of Machine Tools and Manufacture **153**, 103553 (2020).
15. J. Steuben, A. Iliopoulos and J. Michopoulos, "Recent Developments of the Multiphysics Discrete Element Method for Additive Manufacturing Modeling and Simulation," in *Proceedings of the ASME 2017 International Design Engineering Technical Conferences & Computers and Information in Engineering Conference,* American Society of Mechanical Engineers Digital Collection 2017. (Cleveland, Ohio, 2017), pp. 12.
16. R. Ganeriwala and T. Zohdi, Procedia CIRP **14**, 299-304 (2014).
17. M. Turner, R. Clough, H. Martin and L. Topp, Journal of the Aeronautical Sciences **23**, 805-823 (1956).
18. E. Papazoglou, N. Karkalos and A. Markopoulos, The International Journal of Advanced Manufacturing Technology **111**, 2939-2955 (2020).
19. M. Li, Y. Han, M. Zhou, P. Chen, H. Gao, Y. Zhang and H. Zhou, "Experimental investigating and numerical simulations of the thermal behavior and process optimization for selective laser sintering of PA6", Journal of Manufacturing Processes **56**, 271-279 (2020).
20. Q. Yang, P. Zhang, L. Cheng, Z. Min, M. Chyu and A. To, Additive Manufacturing **12**, 169-177 (2016).
21. N. Tolochko, M. Arshinov, A. Gusarov, V. Titov, T. Laoui and L. Froyen, Rapid Prototyping Journal **9**, 314-326 (2003).
22. A. Mokrane, M. Boutaous, and S. Xin, Comptes Rendus Mécanique **346**, 1087-1103 (2018).
23. Z. Wang, W. Yan, W. Liu and M. Liu, Computational Mechanics **63**, 649-661 (2019).
24. R. Paul, S. Anand and F. Gerner, Journal of Manufacturing Science and Engineering **136**, 031009-12 (2014).
25. C. Fu and Y. Guo, Journal of Manufacturing Science and Engineering **136**, 061004-7 (2014).
26. W. King, A. Anderson, R. Ferencz, N. Hodge, C. Kamath, S. Khairallah and A. Rubenchik, Applied Physics Reviews **2**, 041304-26 (2015).
27. E. Denlinger, J. Heigel and P. Michaleris, Proceedings of the Institution of Mechanical Engineers, Part B: Journal of Engineering Manufacture **229**, 1803-1813 (2015).
28. M. Ansari, D. Nguyen and H. Park, Materials **12**, 1272-18 (2019).

29. T. Childs, C. Hauser and M. Badrossamay, Proceedings of the Institution of Mechanical Engineers, Part B: Journal of Engineering Manufacture **219**, 339-357 (2005).
30. K. Dai and L. Shaw, Rapid Prototyping Journal **8**, 270-276 (2002).
31. G. Cervera and G. Lombera. Rapid Prototyping Journal **5**, 21-26 (1999).
32. L. Dong, A. Makradi, S. Ahzi and Y. Remond, Journal of Materials Processing Technology **209**, 700-706 (2009).
33. D. Riedlbauer, M. Drexler, D. Drummer, P. Steinmann and J. Mergheim, Computational Materials Science **93**, 239-248 (2014).
34. P. Peyre, Y. Rouchausse, D. Defauchy and G. Régnier, Journal of Materials Processing Technology **225**, 326-336 (2015).
35. A. Foroozmehr, M. Badrossamay, E. Foroozmehr and S. Golabi, Materials & Design **89**, 255-263 (2016).
36. C. Bierwisch, S. Mohseni-Mofidi, B. Dietemann, M. Grünewald, J. Rudloff and M. Lang, Materials & Design **199**, 109432-15 (2021).
37. F. Osmanlic, K. Wudy, T. Laumer, M. Schmidt, D. Drummer and C. Körner, Polymers **10**,784 (2018).
38. E. Papazoglou, N. Karkalos, P. Karmiris-Obrataski and A. Markopoulos. Archives of Computational Methods in Engineering **29**, 941-973 (2022).
39. Z. Luo and Y. Zhao, Additive Manufacturing **21**, 318-332 (2018).
40. B. Soundararajan, D. Sofia, D. Barletta and M. Poletto, Additive Manufacturing **47**, 102336-27 (2021).
41. B. Schoinochoritis, D. Chantzis and Ko. Salonitis, Proceedings of the Institution of Mechanical Engineers, Part B: Journal of Engineering Manufacture **231**, 96-117 (2017).
42. Additive Manufacturing & 3D Printing Simulation Software | Ansys, Available online: https://www.ansys.com/products/additive (Accessed on 28 October 2022).
43. Design and Engineering Simulation | SIMULIA – Dassault Systemes, Available online: https://www.3ds.com/products-services/simulia/ (Accessed on 28 October 2022).
44. COMSOL - Software for Multiphysics Simulation, Available online: https://www.comsol.com/ (Accessed on 20 January 2023).
45. Fusion 360 with Netfabb | Get Prices & Buy Netfabb | Autodesk, Available online: https://https://www.autodesk.com/products/netfabb/overview (Accessed on 20 January 2023).
46. LIGGGHTS Open Source Discrete Element Method Particle Simulation Code | CFDEM project, Available online: https://www.cfdem.com/liggghts-open-source-discrete-element-method-particlesimulation-code/overview (Accessed on 20 January 2023).
47. LAMMPS Molecular Dynamics Simulator, Available online: https://www.lammps.org/ (Accessed on 20 January 2023).
48. M. Gouge and P. Michaleris, "Chapter 1 - An Introduction to Additive Manufacturing Processes and Their Modeling Challenges" in *Thermo-Mechanical Modeling of Additive Manufacturing*, edited by M. Gouge and P. Michaleris (Butterworth-Heinemann, Oxford, 2018), pp. 3-18.
49. OpenFOAM v1806: New and updated solvers and physics, Available online: https://www.openfoam.com/news/main-news/openfoam-v1806/solver-and-physics (Accessed on 20 January 2023).
50. InterFoam - OpenFOAMWiki, Available online: https://openfoamwiki.net/index.php/InterFoam (Accessed on 20 January 2023).
51. OpenFOAM v6 User Guide: 3.5 Standard solvers, Available online: https://cfd.direct/openfoam/user-guide/v6-standard-solvers/ (Accessed on 20 January 2023).
52. J. Castro, "Numerical Modelling of the Selective Laser Sintering Process," Master's dissertation, University of Minho, 2022.
53. PA 12 - PA2200: Nylon for Industrial 3D Printing | EOS GmbH, available online: https://www.eos.info/en/additive-manufacturing/3d-printing-plastic/sls-polymermaterials/polyamide-pa-12-alumide (accessed on 20 January 2023)
54. P. Amend, C. Pscherer, T. Rechtenwald, T. Frick, and M. Schmidt. Physics Procedia **5**, 561-572 (2010).
55. Nitrogen - Density and Specific Weight vs. Temperature and Pressure, available online: https://www.engineeringtoolbox.com/nitrogen-n2-density-specific-weight-temperature-pressure-d_2039.html (Accessed on 20 January 2023).
56. Nitrogen - Thermal Conductivity vs. Temperature and Pressure, available online: https://www.engineeringtoolbox.com/nitrogen-n2-thermal-conductivity-temperature-pressure-d_2084.html (Accessed on 20 January 2023).

57. Nitrogen Gas - Specific Heat vs. Temperature, available online: https://www.engineeringtoolbox.com/nitrogen-d_977.html (Accessed on 20 January 2023).
58. Nitrogen - Dynamic and Kinematic Viscosity vs. Temperature and Pressure, available online: https://www.engineeringtoolbox.com/nitrogen-n2-dynamic-kinematic-viscosity-temperature-pressure-d_2067.html (Accessed on 20 January 2023).
59. W. Schnell and G. Fischer, Applied Optic **14**, :2058-2059 (1975).
60. G. Vasquez, C. Majewski, B. Haworth and N. Hopkinson, Additive Manufacturing **1,** 127-138 (2014).
61. A. Lopes, A. Sampaio and A. Pontes, Progress in Additive Manufacturing **7**, 683-698 (2022).
62. B. Haworth, N. Hopkinson, D. Hitt and X. Zhong, Rapid Prototyping Journal **19**, 28-36 (2013).
63. L. Verbelen, S. Dadbakhsh, M. Eynde, J. Kruth, B. Goderis and P. Puyvelde, European Polymer Journal **75**, 163-174 (2016).